Northumbria Research Link

Citation: Xu, Weishu, Zhang, Min, Han, Dahai, Ghassemlooy, Zabih, Luo, Pengfei and Zhang, Yongjian (2018) Real-Time 262-Mb/s Visible Light Communication With Digital Predistortion Waveform Shaping. IEEE Photonics Journal, 10 (3). pp. 1-10. ISSN 1943-0655

Published by: IEEE

URL: http://dx.doi.org/10.1109/JPHOT.2018.2829905 <http://dx.doi.org/10.1109/JPHOT.2018.2829905>

This version was downloaded from Northumbria Research Link: http://nrl.northumbria.ac.uk/id/eprint/34281/

Northumbria University has developed Northumbria Research Link (NRL) to enable users to access the University's research output. Copyright © and moral rights for items on NRL are retained by the individual author(s) and/or other copyright owners. Single copies of full items can be reproduced, displayed or performed, and given to third parties in any format or medium for personal research or study, educational, or not-for-profit purposes without prior permission or charge, provided the authors, title and full bibliographic details are given, as well as a hyperlink and/or URL to the original metadata page. The content must not be changed in any way. Full items must not be sold commercially in any format or medium without formal permission of the copyright holder. The full policy is available online: http://nrl.northumbria.ac.uk/policies.html

This document may differ from the final, published version of the research and has been made available online in accordance with publisher policies. To read and/or cite from the published version of the research, please visit the publisher's website (a subscription may be required.)

Northumbria University NEWCASTLE

University Library

Experimental Demonstration of High-Speed 4 × 4 Imaging Multi-CAP MIMO Visible Light Communications

Khald Werfli, Petr Chvojka, Zabih Ghassemlooy*, Navid Bani Hassan, Stanislav Zvanovec, Andrew Burton, Paul Anthony Haigh, and Manav R. Bhatnagar

***Abstract*—In general, visible light communication (VLC) systems, which utilise white light-emitting diodes (LEDs), only offer a bandwidth limited to the lower MHz region. Therefore, providing VLC-based high data rate communications systems becomes a challenging task. To address this challenge, we propose a solution based on multiplexing in both the frequency and space domains. We experimentally demonstrate a 4 × 4 imaging multiple-input multiple-output (MIMO) VLC system (i.e., space multiplexing) utilising multi-band carrier-less amplitude and phase (*m*-CAP) modulation (i.e., frequency multiplexing). Independently, both MIMO and *m*-CAP have shown the remarkable ability to improve transmission speeds in VLC systems, and hence, here we combine them to further improve the net data rate. We investigate link performance by varying the number of subcarriers *m*, link distance *L*, and signal bandwidth B_{sig}. From all the values tested, we show a data rate of ~249 Mb/s can be maximally achieved for for *m* = 20, B_{sig} = 20 MHz, and *L* = 1 m, at a bit error rate of 3.2×10^{-3} using LEDs with ~4 MHz bandwidth.**

***Index Terms*—Modulation bandwidth, multi-band carrier-less amplitude and phase modulation, multiple-input multiple-output, visible light communications.**

I. Introduction

WIRELESS access technologies have continuously evolved in response to ever increasing capacity demands resulting from the wide spread use of smart and mobile devices. Current 4th generation wireless systems with a limited frequency spectrum will not be able to apportion sufficient bandwidth to cope with the exponentially growing traffic, and hence, highly spectrally efficient communication techniques are one of the key considerations in research towards the 5th generation networks [1]. Within this context, visible light communications (VLC) can be used as a complementary wireless technology [2] to radio-frequency based schemes mostly in applications where high bandwidth *B* and low latencies are the main requirements. VLC has received growing research interest over the last decade; mostly due to the widespread use of light emitting diodes (LEDs) in solid-state lighting systems [3]. However, VLC systems have a number of challenges including (*i*) LEDs with limited bandwidths B_{LED} (typically < 5 MHz, or higher for micro-LEDs); (*ii*) LED non-linearity; (*iii*) multipath induced inter-symbol interference (ISI); (*iv*) blocking and shadowing; and (*v*) limited mobility [3, 4], which limits the maximum achievable data rate R_b within a typical indoor environment.

Numerous number of schemes have been proposed to overcome these limitations [5-10]. As for the B_{LED} and ISI limitations, the most widely adopted schemes include pre- and post-equalizations, blue filtering, multiplexing and parallel transmission, and spectrally efficient modulation as well as multi-carrier transmission [11-13]. Of the latter, orthogonal frequency division multiplexing (OFDM) offers spectral efficiency only through compatibility with bit- and power-loading algorithms, thus enabling a higher number of bits/symbol/subcarrier [14, 15]. In [16-18] OFDM VLC links with R_b of several Gb/s were reported, and in [19] the aggregate R_b was increased to 3.4 Gb/s using a combination of OFDM and wavelength division multiplexing (WDM). Despite many advantages that OFDM offers, there are a number of drawbacks including (*i*) limited dynamic range; (*ii*) relatively high peak-to-average power ratio due to the LED nonlinearity [16-18]; and (*iii*) sensitivity to the carrier offset and drift, and phase noise, which results in lower overall spectral efficiency [20-22].

Alternatively, carrier-less amplitude and phase (CAP) modulation was shown to outperform OFDM in terms of R_b over the same transmission span *L* [23]. In [24], a CAP-VLC system employing a red-green-blue (RGB) LED and a hybrid post-equalizer was reported with R_b of 3.22 Gb/s. Overall, the CAP system based on intensity modulation and direct detection is less complex with improved performance compared to OFDM, which allows relatively higher R_b using optical and electrical components with limited *B* [25].

Manuscript received August 30, 2017.

Khald Werfli, Zabih Ghassemlooy, Navid Bani Hassan, and Andrew Burton are with the Optical Communications Research Group, Northumbria University, Newcastle-upon-Tyne NE1 8ST, UK (e-mail: khald.werfli@northumbria.ac.uk; z.ghassemlooy@northumbria.ac.uk; navid.hassan@northumbria.ac.uk; andrew2.burton@northumbria.ac.uk)

* Is with QIEM, Chinese Academy of Sciences, Fujian, China

Petr Chvojka and Stanislav Zvanovec are with the department of Electromagnetic Field, Czech Technical University in Prague, Technicka 2, 16627 Prague, Czech Republic (e-mail: chvojpe8@fel.cvut.cz;; xzvanove@fel.cvut.cz)

Paul Anthony Haigh is with the department of Electronic and Electrical Engineering, University College London, WC1E 6BT, UK (e-mail:p.haigh@ucl.ac.or.uk)

Manav R. Bhatnagar is with the Indian Institute of Technology Delhi, New Delhi, 110016, India (e-mail: manav@ee.ittd.ac.in)

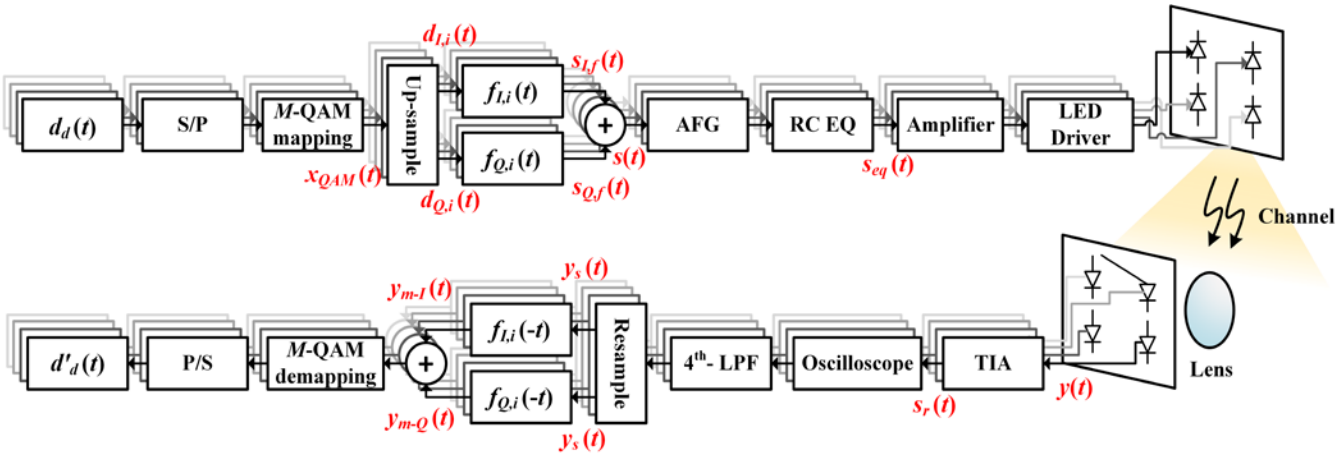

Fig. 1. The schematic block diagram of the 4 x 4 imaging MIMO *m*-CAP system

However, despite superior R_b and bit-error rate (BER) performance in comparison to OFDM, the major impediment in implementation of CAP VLC is that it is very sensitive to the high frequency attenuation [26], which is prevalent in VLC systems due to the LED frequency response (i.e., a low pass filter (LPF)). In [27] multi-band CAP (*m*-CAP) was first proposed for optical fibre communications prior to adoption by the VLC community [26], where the system bandwidth B_{sys} was evenly divided over m = 10 subcarriers, each employing CAP with successively higher carrier frequencies over a low modulation bandwidth. It was found that a higher signal-to-noise ratio (SNR) per subcarrier could be supported due to the alleviation of the band-limiting conditions. Furthermore, the implementation of a bit-loading algorithm, which is not possible in 1-CAP, enabled the demonstration of a record (at the time of writing) spectral efficiency η_s of 4.85 b/s/Hz.

Simultaneously, the multiple-input multiple-output (MIMO) scheme can be adopted to increase the R_b. In indoor environments multiple LED-based lighting fixtures are used to provide sufficient illumination levels (i.e., 200-1000 lx [28]), which facilitates the implementation of MIMO-VLC [29]. An imaging MIMO-VLC system using micro-LEDs (B_{LED} > 20 MHz) and R_b of ~920 Mb/s over L of 1 m was experimentally demonstrated in [30]. In [31] an experimental 4 × 4 optical non-imaging MIMO-VLC link with an aggregate R_b of 50 Mb/s over L of 2 m was demonstrated. In this work, for the first time, we experimentally demonstrate a 4 × 4 imaging MIMO-VLC system based on *m*-CAP (i.e., a combination of frequency- and space-division multiplexing), and investigate the link's BER performance as a function of m (up to 20), a range of signal bandwidth B_{sig} and L. We also examine the net data rate R_{net} and the net spectral efficiency η_{net}; which shows that for a given m and L, increasing B_{sig} leads to an increase in R_{net} and reduced η_{net}. We demonstrate a maximum R_b of ~249 Mb/s at a BER of 3.2×10^{-3}, given m =20, B_{sig} = 20 MHZ and L = 1 m.

The rest of this paper is organised as follows: in Section II the system setup is described; results and discussions are shown in Section III, and finally, conclusions are drawn in Section IV.

II. System Setup

As a proof of concept, Fig. 1 shows the schematic block diagram of the proposed experimental system, where m independent pseudorandom binary sequences (PRBS) $d_d(t)$ in the non-return to zero (NRZ) format of length 2^{17}-1 are generated in the MATLAB domain. Following serial-to-parallel conversion (S/P), $d_d(t)$ is then mapped onto the *M*-ary quadrature amplitude modulation (*M*-QAM) constellation symbols $x_{QAM}(t)$, where the cardinality is given by $M = 2^b$ and b represents the number of bits/symbol. $x_{QAM}(t)$ is then up-sampled by the number of samples/symbol n_{samp} as given by [27]:

$$n_{samp} => 2m(1+\beta), \tag{1}$$

where m represents the number of subcarriers, and β is the roll-off factor of the square root raised cosine (SRRC) filter, which is set to 0.15 for consistency with the literature [26, 27].

Both up-sampled signals $d_{I,i}(t)$ and $d_{Q,i}(t)$ of the i^{th} subcarrier are then passed through the real (I) and imaginary (Q) SRRC filters the outputs of which are given as [26]:

$$s_{I,f,i}(t) = d_{I,i}(t) \otimes f_{I,i}(t), \tag{2}$$

$$s_{Q,f,i}(t) = d_{Q,i}(t) \otimes f_{Q,i}(t), \tag{3}$$

where $\otimes$ denotes time domain convolution, $f_{I,i}(t)$ and $f_{Q,i}(t)$ denote the impulse response of the I and Q SRRC filters of the i^{th} subcarrier, respectively, which are given by [32]:

$$f_{I,i}(t) = \cos\left(2\pi f_{c,i}t\right) \cdot \left[\frac{\sin\left(\frac{\pi t}{T_s}(1-\beta)\right) + 4\beta\frac{t}{T_s}\cos\left(\frac{\pi t}{T_s}(1+\beta)\right)}{\frac{\pi t}{T_s}\left(1-\left(4\beta\frac{t}{T_s}\right)^2\right)}\right], \tag{4}$$

$$f_{Q,i}(t) = \sin\left(2\pi f_{c,i}t\right) \cdot \left[\frac{\sin\left(\frac{\pi t}{T_s}(1-\beta)\right) + 4\beta\frac{t}{T_s}\cos\left(\frac{\pi t}{T_s}(1+\beta)\right)}{\frac{\pi t}{T_s}\left(1-\left(4\beta\frac{t}{T_s}\right)^2\right)}\right], \tag{5}$$

where T_s is the symbol duration. The carrier frequency for the i^{th} subcarrier is given by [33]:

$$f_{c,i} = \frac{(2i-1)B_{sig}}{2m}, \tag{6}$$

where B_{sig} is given by:

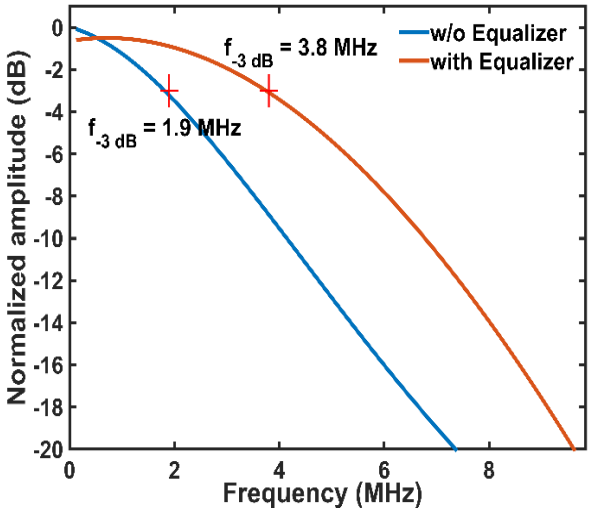

Fig. 3. LED frequency response with and without an equalizer

$$B_{sig} = \frac{1}{T_s}(1+\beta)m. \tag{7}$$

Considering all subcarriers, the m-CAP output signal is given as [32]:

$$s(t) = \sqrt{2}\left(s_{I,f}(t) - s_{Q,f}(t)\right). \tag{8}$$

The m-CAP signal is then applied to identical arbitrary function generators (AFGs) using LabVIEW to generate the signals for the 4 spatial channels. The outputs $s(t)$ of the four channels are sampled at 2 GS/s with a vertical resolution of 8-bit and is then passed through four independent resistor-capacitor based pre-equalizers (RC EQ) in order to extend B_{LED} from ~2 MHz to 3.8 MHz, as shown in Fig. 2.

The four equalised signals $s_{eq}(t)$ are then amplified (with a gain of 5 dB) prior to intensity modulation of LEDs (4 cool white 565K LUXEON Rebel LEDs) using a bias tee. Fig. 3 illustrates the experimental setup of the proposed system.

Note, the distances between the transmitter (Tx) and the lens L_t and between the lens and the optical receiver (Rx) L_r, respectively are given as:

$$L_t = f_l\frac{(\alpha-1)}{\alpha}, \tag{9}$$

$$L_r = f_l(1-\alpha), \tag{10}$$

where f_l is the lens focal length with a magnification factor given by [34]:

$$\alpha = -\frac{d_r}{d_t} = -\frac{L_r}{L_t}, \tag{11}$$

where d_r and d_t are the spacing between Rxs and Txs, respectively.

Using the parameters given in Table I, the total link span $L = L_t + L_r = 4.5f_l$. For f_l of 0.25, 0.4 and 1 m, L are 1.125 m, 1.8 m and 4.5 m, respectively, which are representative dimensions for a typical indoor environment.

As shown in Fig. 3, at the Rx, a convex lens with a focal length $\boldsymbol{f_l}$ is used to focus the received optical beam of each channel onto its corresponding photodetectors (PDs) (silicon

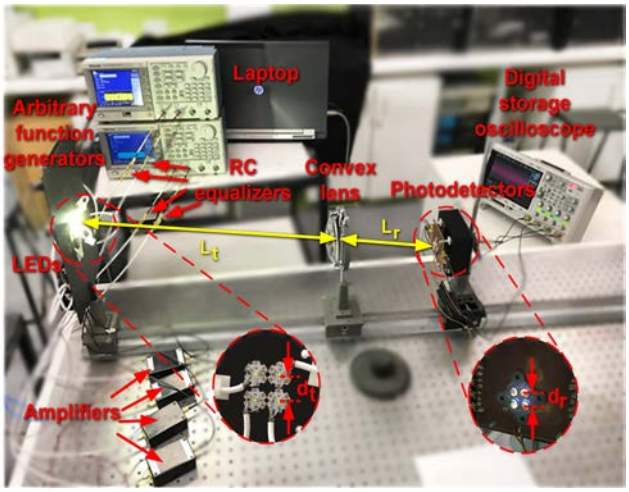

Fig. 2. Experimental setup. The convex lens is used to map the LEDs to the PDs. Spacing between Rxs and Txs d_r and d_t, respectively

PD OSD15-5T) with a large enough surfacing area to capture the entire optical foot print. Therefore, with the proposed system being an imagining MIMO the lens employed at the Rx ensures that each PD receives the optical signal from its corresponding LED. As a result there are no inter-channel crosstalk as in [35], in contrast to the non-imaging MIMO VLC system, where additional signal processing and filtering are needed to mitigate the channel correlation between individual Txs and Rxs, and inter-channel crosstalk.[35].

The received signal is given by:

Table I: SETUP AND PD PARAMETERS

Parameter	**Value**
Data-NRZ pseudorandom binary sequences length	2^{17}-1
Amplifier gain	5 dB
Convex lens	
• Focal length f_l	0.25 m, 0.40 m and 1 m
• Diameter d	110 mm, 105 mm and 50 mm
LED bandwidth B_{LED}	1.9 MHz
Photodetector - silicon OSD15-5T	
• Active area	15 mm^2
• Responsivity $\mathcal{R}$	0.21 A/W
• Bandwidth B_{PD}	29 MHz
Spacing between Txs d_t	0.01 m
Spacing between Rxs d_r	0.02 m
Signal bandwidth B_{sig}	5,10,15 and 20 MHz
Transmission span L	~1 m, 1.8 m and 4.5 m

$$y(t) = \mathcal{R}s_{eq}(t) \otimes h(t) + n(t), \quad (12)$$

where $h(t)$ is the channel impulse response, $\mathcal{R}$ represents the PD's responsivity, and $n(t)$ is the additive white Gaussian noise (AWGN). Note, the dominant noise sources are the ambient induced shots noise and the thermal noise, which are defined, respectively in terms of variances and is given as [28]:

$$\sigma_n^2 = 2qI_{bg}B_{Rx} + 4kTB_{Rx}, \quad (13)$$

where I_{bg} is the background light induced current, q is the electron charge, T is the absolute temperature, k is the Boltzmann's constant, and B_{Rx} is the receiver bandwidth.

A typical value for the thermal noise σ_{ther}^2 = 17.5348×10^{-16} A^2 [36]. For a typical indoor environment the standard illumination level is between 300 - 500 lx at 0.8 m height from the floor level, which is equivalent to a power requirement of > 2.25×10^{-4} W [36]. This represents the shot noise variance of at least ~2×10^{-16} A^2, which is the same as σ_{ther}^2.

Following optoelectronic conversion and amplification using transimpedance amplifiers (TIAs), the regenerated electrical signals $s_r(t)$ are captured using a digital storage oscilloscope (DSO-X3034A) with a sampling rate of 4 GS/s for off-line processing as outlined in the following paragraphs. $s_r(t)$ is first passed through a 4th order Butterworth LPF with a cut-off frequency f_{cut} = B_{sig} [26] in order to reject the out-of-band noise. The filtered *m*-CAP signal is then resampled to match the transmitted sampling frequency prior to matched filtering, the output of which is given by:

$$y_{m-I}(t) = y_s(t) \otimes f_{I,i}(-t), \quad (14)$$

$$y_{m-Q}(t) = y_s(t) \otimes f_{Q,i}(-t), \quad (15)$$

where $y_s(t)$ is the resampled signal. $f_I(-t)$ and $f_Q(-t)$ are the impulse responses of the matched filters.

Following *M*-QAM demodulation and parallel-to-serial conversion (P/S) the estimated data symbols $d'_{\mathrm{d}}(t)$ are recovered. As reported in the literature, a binary phase shift keying based signal is first transmitted on each subcarrier to measure the error vector magnitude (EVM), prior to SNR estimation following the procedures adopted from [37, 38]:

$$\mathrm{SNR}_i = 20\log_{10}\left(\frac{\mathrm{EVM}_{\mathrm{RMS}_i}(\%)}{100}\right). \quad (16)$$

Next, a subcarrier-specific value of *b* is selected based on the estimated SNR. The proposed system performance is then assessed in terms of (*i*) R_b as a function of *m*; and (*ii*) the assigned *b* versus the order of *m*. Here, we have adopted the target BER of 10^{-3} allowing a margin for the 7% forward error correction limit (FEC), which has a BER limit of 3.8×10^{-3} [39]. The SNR$_{\text{threshold}}$ for the targeted BER can be found as the literature [40]. Therefore, at the target BER we defined a set of values for SNR$_{\text{threshold}}$ of {6.8, 9.8, 16.6, 22.6, 28.5} dB for *b* = {1, 2, 4, 6, 8}, respectively.

Note that, the reported net data rate $R_{net} = \sum_i^N R_{b,i}$, where *N* is the channels (i.e., 4 in this case)) with no 7% FEC overhead. Through sequential isolation of the LEDs, we measured that the inter-channel crosstalk to be < 0.2 dB, therefore the individual channels can be considered as a single-input single-output (SISO) link.

Following the above procedure, the *m*-CAP signals are transmitted and the BER is determined by comparing $d'_d(t)$ and $d_d(t)$.

III. Results and Discussions

In this section, we outline experimental evaluation of a 4 × 4 optical imaging MIMO-VLC utilising the *m*-CAP scheme by investigating the impact of using (*i*) different B_{sig}, while maintaining a fixed *L* of ~1 m; (*ii*) a range of subcarriers *m* up to 20 and B_{sig} of 5, 10, 15 and 20 MHz for *L* of ~1 m at the adopted BER target of 10^{-3}; and (*iii*) a range of *L* = ~1, 1.8 and 4.5 m and $m = \{20, 15, 10, 5\}$ for B_{sig} of 10 MHz.

A. Signal bandwidth B_{sig}

Fig. 4(a) illustrates R_{net} as a function of *m* for a range of B_{sig}, for *L* of ~1 m and a BER of 10^{-3}. Note, 20-CAP displays the highest R_{net} of ~249 Mb/s (the highest reported in this work) at a BER of 3.2×10^{-3} for B_{sig} = 20 MHz, which reduces to ~121 Mb/s for B_{sig} = 5 MHz. At the B_{sig} of 5 MHz, the increase in R_{net} as a function of *m* is relatively small since all the subcarriers have a similar bandwidth per subcarrier B_{sc}. For the B_{sig} of 20 MHz, the drop in R_{net} is due to reduced B_{sc} for a given *m* and B_{sig}. For example, for *m* = 20 and B_{sig} = 20 MHz, the B_{sc} is 1 MHz, whereas, for *m* = 20 and B_{sig} = 5 MHz, B_{sc} reduces to 0.25 MHz. For B_{sig} of 15 and 10 MHz, R_{net} reaches 237.75 Mb/s and 213.49 Mb/s, respectively. Moreover, for higher values of B_{sig} (e.g., 20 MHz and *m* = 20) the out of band subcarriers can still be loaded with *b* = 4 starting from the 7th subcarrier as shown in Fig. 4(b), which depicts the assigned *b* values for 20-CAP and for a range of B_{sig} {20, 15, 10 and 5 MHz}.

Using a range of B_{sig} (i.e., 20, 15, 10 and 5 MHz) for *m* = 20, we observe η_{net} of 12.45, 15.85, 21.34, 24.26 b/s/Hz, respectively. This is interesting as it shows that using higher B_{sig} leads to less utilisation of the spectrum but higher R_{net}. Moreover, for *m* = 20 and B_{sig} of 5, 10 and 15 MHz we observe an improvement in η_{net} of ~95%, ~72% and ~27% compared to *m* = 20 and B_{sig} of 20 MHz. Hence, there is a trade-off between the achievable R_{net} and spectral utilisation when considering different values of B_{sig} for the same *m*-CAP system. This can be attributed to the fact B_{sc} increases with B_{sig} since the subcarriers are divided equally, which leads to reduced SNR of each individual subcarrier positioned outside the pass-band region (i.e., the roll-off region of the LPF response of the LED with 20 dB/decade). Therefore, they are assigned with a low *b* value (see Fig. 4(b)). However, due to the increase in B_{sig} the R_{net} is boosted as it increases proportionally with B_{sig} (i.e., $\frac{1}{T_S}(1+\beta)m$). Moreover, $R_{net} = \sum_{i=1}^{m} k_i \frac{1}{T_s}$ for all four channels in addition to removal of the 7% FEC overhead. In contrast, for a given *m* decreasing B_{sig} leads to a higher SNR per subcarrier, which is due to lower B_{sc} that ensures higher *b* values (Fig. 4(b)). Therefore, achieving higher spectral utilisation for a given B_{sig}.

In Table II we have summarised the results in a tabular form for simplicity.

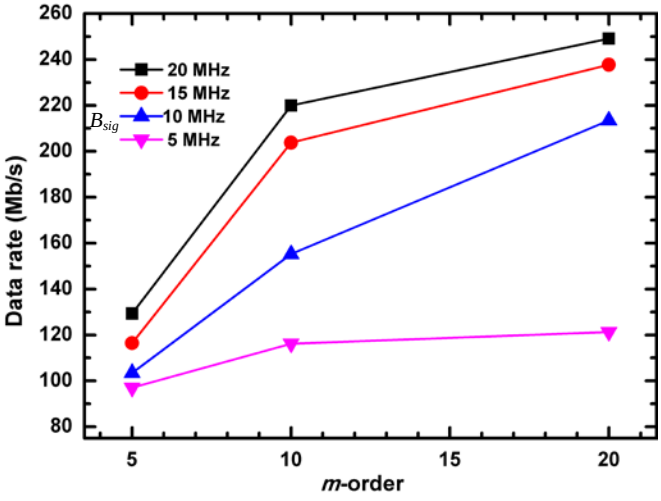

(a)

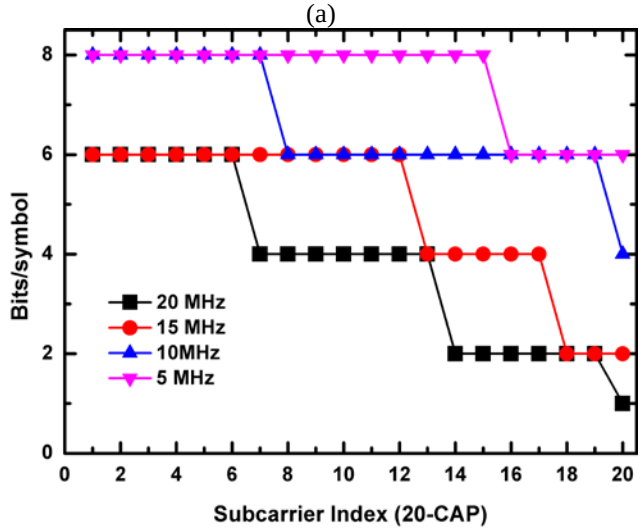

(b)

Fig. 4. (a) The net data rate R_{net} against m for a range of B_{sig}, and a BER of 10^{-3}, and (b) assigned bits/symbol for 20-CAP for a range of B_{sig} (20, 15, 10 and 5 MHz). Note, in (b) the highest value of b = 8 is assigned for the first 7th and 15th subcarriers with B_{sig} of 10 and 5 MHz, respectively, since they are within B_{LED}

Table II: SUMMARY OF THE ACHIEVED R_{net} AND η_{net} FOR A RANGE OF B_{sig} AND m

m \ B_{sig}	5 MHz	10 MHz	15 MHz	20 MHz
5	97.03 Mb/s 19.4 b/s/Hz	103.5 Mb/s 10.35 b/s/Hz	116.44 Mb/s 7.76 b/s/Hz	129.39 Mb/s 6.46 b/s/Hz
10	116.25 Mb/s 23.25 b/s/Hz	155.26 Mb/s 15.52 b/s/Hz	203.79 Mb/s 13.58 b/s/Hz	219.96 Mb/s 11 b/s/Hz
20	121.31 Mb/s 24.26 b/s/Hz	213.49 Mb/s 21.34 b/s/Hz	237.75 Mb/s 15.85 b/s/Hz	249.07 Mb/s 12.45 b/s/Hz

In order to demonstrate the performance of SISO under the same conditions as the imaging MIMO, R_{net} for a range of m = {20, 15, 10, 5}, L of ~1 m and a target BER of 10^{-3} for one of the channels (i.e., Ch1) is shown in Fig. 5. Note that, as stated earlier all four channels in MIMO have the same data rate therefore, each channel can be considered as a SISO link. As illustrated in Fig. 5, the highest R_{net} that can be supported by a SISO link is 62.26 Mb/s for m = 20 and B_{sig} = 20 MHz. For B_{sig} = 5 MHz the R_{net} drops to 24.25 Mb/s, which is the lowest value reported for a SISO link. A summary of the achieved results for the SISO link for a range of m and B_{sig} is given in the Table III.

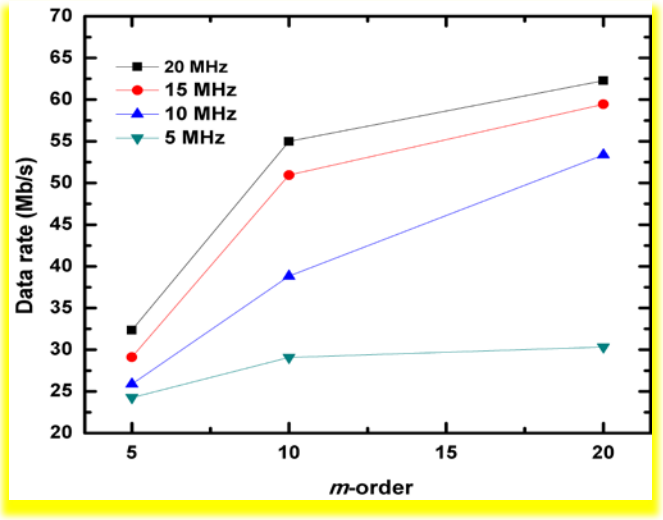

Fig. 5. The net data rate R_{net} against m for a range of B_{sig} for SISO (Ch1)

Figs. 6(a) and (b) depict the measured frequency spectra of the 20-CAP system for the B_{sig} of 20 MHz and the corresponding constellation diagrams of the 1st (black), 7th (red), and 14th (green) subcarriers, respectively. From Fig. 5(a) the 1st six subcarriers occupy a bandwidth of 6 MHz. Note, EVM_{RMS} values for the three constellations shown are 5.11%, 7.31% and 15.73%, respectively. Fig. 7 then illustrates the spectral efficiency as a function of m for the range of B_{sig}. Note, from Fig. 4(a) for m = 10 and B_{sig} of 20, 15, 10 and 5 MHz, the R_{net} that can be supported are 219.96, 203.79, 155.26 and 116.25 Mb/s, respectively. This corresponds to η_{net} of 11, 13.58, 15.52 and 23.25 b/s/Hz for the listed B_{sig}. Moreover, improved spectral utilisation of ~130%, ~54% and 34.45% for B_{sig} of 5, 10 and 15 MHz, respectively, is obtained in contrast to the B_{sig} of 20 MHz. For m = 5 and B_{sig} of 20, 15, 10 and 5 MHz, η_{net} values are reduced to 6.46, 7.76, 10.35 and 19.4 b/s/Hz, respectively. Alternatively, for B_{sig} of 5, 10, and 15 MHz and m of 5 we observe corresponding improvement in the spectrum utilisation of 203% ~60% and ~74% compared to the B_{sig} of 20 MHz.

At this stage, it is worth mentioning that by combining both space multiplexing (MIMO) and frequency multiplexing (m-CAP) schemes, the overall system transmission speed is improved by ~8 times from 31.53 Mb/s to ~249 Mb/s in contrast to [26]. To the best of authors' knowledge this is the only experimental work on implementation of m-CAP (up to 10) in the VLC domain reported in the literature. We have kept L to be ~1 m. However, in this work B_{sig} is increased by ~3 times, which is higher than the 6.5 MHz adopted in [26]. It should be noted that, the aim of this paper is not to achieve the highest value in R_{net}, but to demonstrate the possible gain that

can be achieved by combining space and frequency

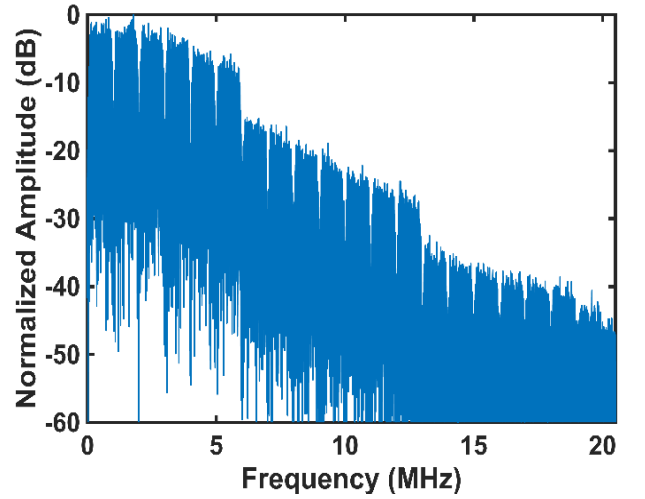

(a)

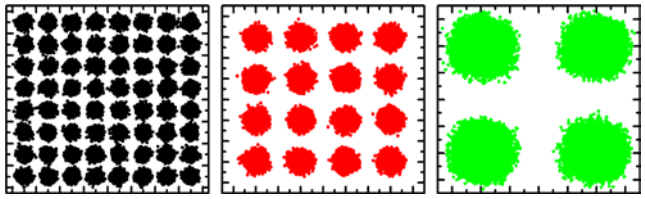

(b)

Fig. 6. 20-CAP with B_{sig} of 20 MHz; (a) the measured frequency spectrum, and (b) constellation diagrams for the 1st, 7th and 14th subcarriers

multiplexing schemes.

Table III: SUMMARY OF SISO's ACHIEVED R_{net} AND η_{net} FOR DIFFERENT B_{sig} AND A RANGE OF m

m \ B_{sig}	5 MHz	10 MHz	15 MHz	20 MHz
5	24.25 Mb/s 4.85 b/s/Hz	25.87 Mb/s 2.58 b/s/Hz	29.11 Mb/s 1.94 b/s/Hz	32.34 Mb/s 1.61 b/s/Hz
10	29.06 Mb/s 5.81 b/s/Hz	38.81 Mb/s 3.88 b/s/Hz	50.94 Mb/s 3.39 b/s/Hz	55 Mb/s 2.75 b/s/Hz
20	30.32 Mb/s 6.07 b/s/Hz	53.37 Mb/s 5.33 b/s/Hz	59.43 Mb/s 3.96 b/s/Hz	62.26 Mb/s 3.11 b/s/Hz

Moreover, in order to increase R_{net} we have doubled the m-order to 20, but at the cost of increased computational complexity of the overall system, since for every increment in m, 2 more pulse shaping FIR filters (i.e., one each for I and Q) are required at both the Tx and the Rx. Note, increasing m from 10 to 20 will lead to the increase of the number of convolution operations from 460 to 1840 at the Tx. For MIMO-VLC m-CAP with m = 10, R_{net} is increased to 213.49 Mb/s compared to 31.53 Mb/s [26] (i.e., a factor of 6.77) over the same L of 1 m. Increasing B_{sig} to 10 MHz results in η_{net} being increased by a factor of 4.4 as the obtained η_{net} is 21.34 b/s/Hz compared to 4.85 b/s/Hz in [26], which is considerable in VLC.

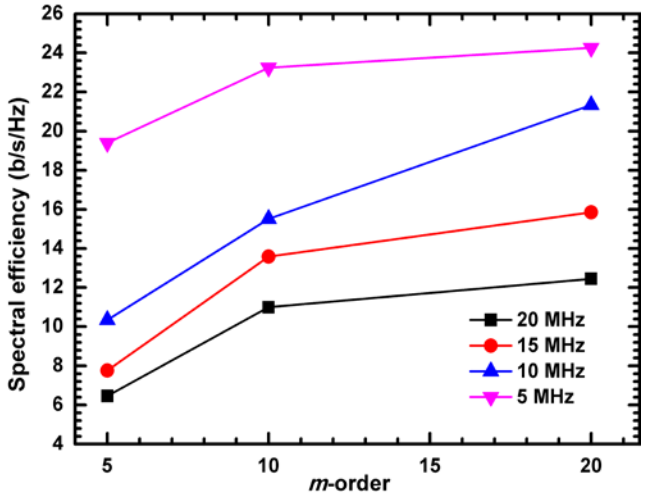

Fig. 7. The spectral efficiency against m for a range of B_{sig} {20, 15, 10 and 5 MHz}

B. Transmission span

Fig. 8 illustrates R_{net} as a function of L for a range of m = {20, 15, 10, 5} and the B_{sig} of 10 MHz. In addition, the illuminance values at the Rx for the targeted L are also depicted in the figure. As expected, the illuminance value drops as L increases. The measured recorded illuminance values of 545, 190 and 82 lx are for L = ~1, 1.8 and 4.5 m. As expected, with the increasing L from 1 to 4.5 m has reduced R_{net} from 213 Mb/s to approximately 50 Mb/s for 20-CAP. Therefore for 20-CAP this results in η_{net} of 21.35 b/s/Hz and 5 b/s/Hz for the BER values of 1.2×10^{-3} and 3.7×10^{-3}, respectively. For a range of m = {20, 15, 10, 5} and L of ~1 m R_{net} values are 213.49, 181.14, 155.26 and 116.44 Mb/s, respectively; where the corresponding values of η_{net} are 21.35, 18.11, 15.52 and 11.64 b/s/Hz. Finally, Fig. 9 outlines the achievable BER performance as a function of L for a range of m. As expected, the BER increases with L and m, reaching 3.7×10^{-3}, which is still below the 7% FEC limit of 3.8×10^{-3} for m = 20 and L of 4.5 m.

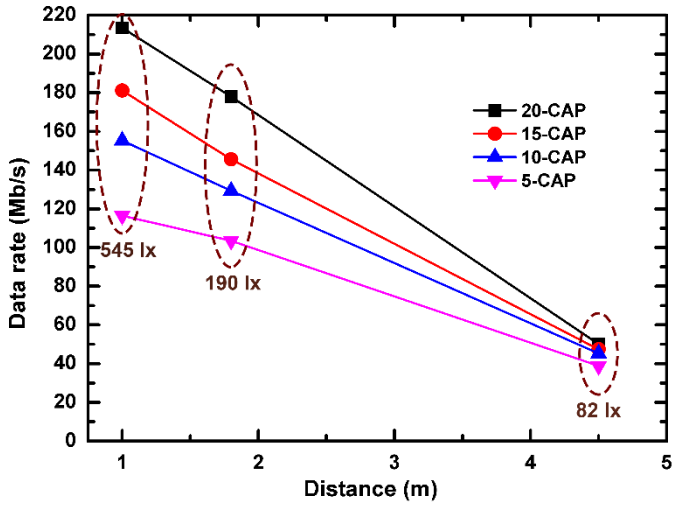

Fig. 8. The measured net data rate R_{net} as a function of the transmission distance for B_{sig} of 10 MHz and a range of m-CAPs. Illuminance values at the Rx for the tested transmission distances are also labelled in the figure

By extending L to 1.8 m, R_{net} is dropped to 177.9, 145.56, 129.39 and 103.5 Mb/s (see Fig. 8), which corresponds to a reduction in η_{net} of 17.79, 14.55, 12.94 and 10.35 b/s/Hz. The highest BER achieved for the L of 1.8 m is 2.6×10^{-3} at m = 20 (see Fig. 9); following the same upward trend as in m and L.

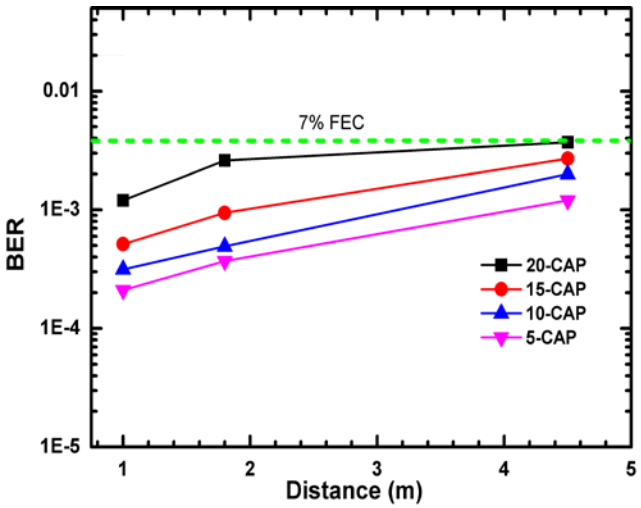

Fig. 9. The measured BER as a function of the distances for different values of *m*; also included is the 7% FEC limit (dashed green)

For the highest L of 4.5 m, R_{net} is reduced (refer to Fig. 8) compared to the shorter distances, with R_{net} of 50.13, 47.43, 45.28 and 38.81 Mb/s at m = {20, 15, 10, 5}, respectively. Similar values of R_{net} are observed for lower values of b for each subcarrier. In other words, the bit loading algorithm fails to introduce any improvement in the overall R_{net} as a result of all subcarriers having low SNR values (i.e., ≪16.6 dB; which is the $SNR_{threshold}$ at b = 4). Also, a reduction in the spectral efficiency was observed and for the first time in this work, it fell below 5 b/s/Hz. A summary of the achieved results for a set of L and m is provided in a tabular form for simplicity (see Table IV)

Table IV: SUMMARY OF THE ACHIEVED R_{net} AND η_{net} FOR A RANGE OF L AND m

m \ *L*	~1 m	1.8 m	4.5 m
5	116.44 Mb/s 11.64 b/s/Hz	103.5 Mb/s 10.35 b/s/Hz	38.81 Mb/s 3.88 b/s/Hz
10	155.26 Mb/s 15.52 b/s/Hz	129.39 Mb/s 12.94 b/s/Hz	45.28 Mb/s 4.52 b/s/Hz
15	181.14 Mb/s 18.11 b/s/Hz	145.56 Mb/s 14.55 b/s/Hz	47.43 Mb/s 4.74 b/s/Hz
20	213.49 Mb/s 21.35 b/s/Hz	177.9 Mb/s 17.79 b/s/Hz	50.13 Mb/s 5 b/s/Hz

IV. CONCLUSION

In this paper, we have reported for the first time, an investigation of the performance of a 4 × 4 m-CAP imaging MIMO (i.e., frequency and space multiplexing) VLC link considering a range of system parameters. By combining the two schemes, we experimentally demonstrated an improvement in the transmission speed reaching a maximum value of ~249 Mb/s. We showed that there is a trade-off between R_{net} and η_{net}, since for a given values of m and L increasing B_{sig} substantially improved R_{net}; however, interestingly η_{net} was reduced. Moreover, the highest R_{net} of 249.07 Mb/s was achieved at a BER of 3.2×10^{-3} for B_{sig} of 20 MHz and for m = 20 over a transmission span of ~1 m. On the other hand, for lower B_{sig} of 5 MHz and for m = 20 the achieved R_{net} was reduced to 121.21 Mb/s, but spectrum utilisation was almost 95% better in contrast to B_{sig} of 20 MHz. We also observed that for a given value of m and B_{sig}, increasing the distance resulted in reduced R_{net}. The overall R_{net} (η_{net}) for all proposed system (i.e., four channels) were 213.49 Mb/s (21.35 b/s/Hz), 177.9 Mb/s (17.79 b/s/Hz), and 50.13 Mb/s (5.01 b/s/Hz) for m = 20 and the B_{sig} of 10 MHz over a range of L (i.e., ~1 m, 1.8 m and 4.5 m), respectively, at BER values of 1.2×10^{-3}, 2.6×10^{-3}, and 3.7×10^{-3}.

Moreover, we showed that for the highest L of 4.5 m increasing m did not introduce any significant improvement in the system performance, but increased the computational complexity by the way of increased number of the pulse shaping FIR filters. In our future work, we will experimentally compare the m-CAP and OFDM schemes performance.

ACKNOWLEDGEMENTS

This work was supported by the UK EPSRC grant EP/P006280/1: Multifunctional Polymer Light-Emitting Diodes with Visible Light Communications (MARVEL) and the GACR 17-17538S.

REFERENCES

[1] C. X. Wang *et al.*, "Cellular architecture and key technologies for 5G wireless communication networks," *IEEE Communications Magazine*, vol. 52, no. 2, pp. 122-130, 2014.

[2] S. Zvanovec, P. Chvojka, P. A. Haigh, and Z. Ghassemlooy, "Visible Light Communications towards 5G," *Radioengineering*, vol. 24, no. 1, pp. 1-9, 2015.

[3] Z. Ghassemlooy, L. N. Alves, S. Zvanovec, and M. A. Khalighi, *Visible Light Communications: Theory and Applications*. Boca Raton: CRC Press, 2017.

[4] Z. Ghassemlooy, S. Arnon, M. Uysal, Z. Xu, and J. Cheng, "Emerging Optical Wireless Communications-Advances and Challenges," *IEEE Journal on Selected Areas in Communications*, vol. 33, no. 9, pp. 1738-1749, 2015.

[5] H. L. Minh *et al.*, "100-Mb/s NRZ Visible Light Communications Using a Postequalized White LED," *IEEE Photonics Technology Letters*, vol. 21, no. 15, pp. 1063-1065, 2009.

[6] P. A. Haigh *et al.*, "Exploiting Equalization Techniques for Improving Data Rates in Organic Optoelectronic Devices for Visible Light Communications," *Journal of Lightwave Technology*, vol. 30, no. 19, pp. 3081-3088, 2012.

[7] P. A. Haigh, Z. Ghassemlooy, S. Rajbhandari, I. Papakonstantinou, and W. Popoola, "Visible Light Communications: 170 Mb/s Using an Artificial Neural Network Equalizer in a Low Bandwidth White Light Configuration," *Journal of Lightwave Technology*, vol. 32, no. 9, pp. 1807-1813, 2014.

[8] A. M. Khalid, G. Cossu, R. Corsini, P. Choudhury, and E. Ciaramella, "1-Gb/s Transmission Over a Phosphorescent White LED by Using Rate-Adaptive Discrete Multitone Modulation," *IEEE Photonics Journal*, vol. 4, no. 5, pp. 1465-1473, 2012.

[9] L. Grobe *et al.*, "High-speed visible light communication systems," *IEEE Communications Magazine*, vol. 51, no. 12, pp. 60-66, 2013.

[10] C. L. Liao, Y. F. Chang, C. L. Ho, and M. C. Wu, "High-Speed GaN-Based Blue Light-Emitting Diodes With Gallium-Doped ZnO

Current Spreading Layer," *IEEE Electron Device Letters*, vol. 34, no. 5, pp. 611-613, 2013.

[11] D. Tsonev *et al.*, "A 3-Gb/s Single-LED OFDM-Based Wireless VLC Link Using a Gallium Nitride μLED," *IEEE Photonics Technology Letters*, vol. 26, no. 7, pp. 637-640, 2014.

[12] P. A. Haigh *et al.*, "A 20-Mb/s VLC Link With a Polymer LED and a Multilayer Perceptron Equalizer," *IEEE Photonics Technology Letters*, vol. 26, no. 19, pp. 1975-1978, 2014.

[13] J.-Y. Sung, C.-W. Chow, and C.-H. Yeh, "Is blue optical filter necessary in high speed phosphor-based white light LED visible light communications?," *Optics express*, vol. 22, no. 17, pp. 20646-20651, 2014.

[14] S. D. Dissanayake and J. Armstrong, "Comparison of ACO-OFDM, DCO-OFDM and ADO-OFDM in IM/DD Systems," *Journal of Lightwave Technology*, vol. 31, no. 7, pp. 1063-1072, 2013.

[15] Y.-F. Yin, W.-Y. Lan, Y.-H. Hsu, Y.-F. Hsu, C.-H. Wu, and J. Huang, "High-speed modulation from the fast mode extraction of a photonic crystal light-emitting diode," *Journal of Applied Physics*, vol. 119, no. 1, p. 013103, 2016.

[16] D. Bykhovsky and S. Arnon, "An Experimental Comparison of Different Bit-and-Power-Allocation Algorithms for DCO-OFDM," *Journal of Lightwave Technology*, vol. 32, no. 8, pp. 1559-1564, Apr 15 2014.

[17] J. Armstrong, "OFDM for Optical Communications," *Journal of Lightwave Technology*, vol. 27, no. 3, pp. 189-204, 2009.

[18] G. Cossu, A. Wajahat, R. Corsini, and E. Ciaramella, "5.6 Gbit/s Downlink and 1.5 Gbit/s Uplink Optical Wireless Transmission at Indoor Distances (≥ 1.5 m)," in *Optical Communication (ECOC), 2014 European Conference on*, 2014, pp. 1-3.

[19] G. Cossu, A. M. Khalid, P. Choudhury, R. Corsini, and E. Ciaramella, "3.4 Gbit/s visible optical wireless transmission based on RGB LED," (in eng), *Opt Express*, vol. 20, no. 26, pp. B501-6, Dec 10 2012.

[20] L. Chen, B. Krongold, and J. Evans, "Theoretical Characterization of Nonlinear Clipping Effects in IM/DD Optical OFDM Systems," *IEEE Transactions on Communications*, vol. 60, no. 8, pp. 2304-2312, 2012.

[21] H. Ochiai and H. Imai, "Performance analysis of deliberately clipped OFDM signals," *IEEE Transactions on Communications*, vol. 50, no. 1, pp. 89-101, 2002.

[22] T. Jiang and Y. Wu, "An Overview: Peak-to-Average Power Ratio Reduction Techniques for OFDM Signals," *IEEE Transactions on Broadcasting*, vol. 54, no. 2, pp. 257-268, 2008.

[23] F. M. Wu *et al.*, "Performance Comparison of OFDM Signal and CAP Signal Over High Capacity RGB-LED-Based WDM Visible Light Communication," *IEEE Photonics Journal* vol. 5, no. 4, pp. 7901507-7901507, 2013.

[24] W. Fang-Ming, L. Chun-Ting, W. Chia-Chien, C. Cheng-Wei, C. Zhen-Yu, and H. Hou-Tzu, "3.22-Gb/s WDM visible light communication of a single RGB LED employing carrier-less amplitude and phase modulation," in *2013 Optical Fiber Communication Conference and Exposition and the National Fiber Optic Engineers Conference (OFC/NFOEC)*, 2013, pp. 1-3.

[25] L. Tao, Y. Wang, Y. Gao, A. P. T. Lau, N. Chi, and C. Lu, "Experimental demonstration of 10 Gb/s multi-level carrier-less amplitude and phase modulation for short range optical communication systems," *Optics express*, vol. 21, no. 5, pp. 6459-6465, 2013.

[26] P. A. Haigh *et al.*, "A Multi-CAP Visible Light Communications System with 4.85 b/s/Hz Spectral Efficiency," *IEEE Journal on Selected Areas in Communications*, vol. 33, no. 99, pp. 1771-1779, 2015.

[27] M. I. Olmedo *et al.*, "Multiband Carrierless Amplitude Phase Modulation for High Capacity Optical Data Links," *Journal of Lightwave Technology*, vol. 32, no. 4, pp. 798-804, 2014.

[28] Z. Ghassemlooy, W. Popoola, and S. Rajbhandari, *Optical wireless communications: system and channel modelling with Matlab®*. CRC Press, 2012.

[29] P. A. Haigh *et al.*, "A MIMO-ANN system for increasing data rates in organic visible light communications systems," in *2013 IEEE International Conference on Communications (ICC)*, 2013, pp. 5322-5327.

[30] S. Rajbhandari *et al.*, "Imaging-MIMO Visible Light Communication System using μLEDs and Integrated Receiver," in *2014 IEEE Globecom Workshops (GC Wkshps)*, 2014, pp. 536-540.

[31] A. Burton, H. L. Minh, Z. Ghassemlooy, E. Bentley, and C. Botella, "Experimental Demonstration of 50-Mb/s Visible Light Communications Using 4 × 4 MIMO," *IEEE Photonics Technology Letters*, vol. 26, no. 9, pp. 945-948, 2014.

[32] J. Zhang, J. Yu, F. Li, N. Chi, Z. Dong, and X. Li, "11× 5× 9.3 Gb/s WDM-CAP-PON based on optical single-side band multi-level multi-band carrier-less amplitude and phase modulation with direct detection," *Optics express*, vol. 21, no. 16, pp. 18842-18848, 2013.

[33] P. A. Haigh *et al.*, "Multi-band carrier-less amplitude and phase modulation for highly bandlimited visible light communications; Invited paper," in *Wireless Communications & Signal Processing (WCSP), 2015 International Conference*, 2015, pp. 1-5.

[34] N. Giordano, *College Physics*. Nelson Education, 2012.

[35] T. Q. Wang, Y. A. Sekercioglu, and J. Armstrong, "Hemispherical lens based imaging receiver for MIMO optical wireless communications," in *Globecom Workshops (GC Wkshps), IEEE*, 2012, pp. 1239-1243.

[36] Y. Chen, C. W. Sung, S.-W. Ho, and W. S. Wong, "BER analysis for interfering visible light communication systems," in *Communication Systems, Networks and Digital Signal Processing (CSNDSP), 2016 10th International Symposium on IEEE*, 2016, pp. 1-6.

[37] R. Schmogrow *et al.*, "Error Vector Magnitude as a Performance Measure for Advanced Modulation Formats," *IEEE Photonics Technology Letters*, vol. 24, no. 1, pp. 61-63, 2012.

[38] R. A. Shafik, M. S. Rahman, and A. R. Islam, "On the Extended Relationships Among EVM, BER and SNR as Performance Metrics," in *2006 International Conference on Electrical and Computer Engineering*, 2006, pp. 408-411.

[39] J. G. Proakis, *Digital Communications*. New York: McGraw-Hill, 2004.

[40] B. Sklar, *Digital communications*. Prentice Hall Upper Saddle River, 2001.